

High harmonic generation in triangular graphene quantum dots

B.R. Avchyan, A.G. Ghazaryan,* K.A. Sargsyan, and Kh.V. Sedrakian

Centre of Strong Fields, Yerevan State University, 1 A. Manukian, Yerevan 0025, Armenia

(Dated: January 7, 2022)

Higher harmonic generation in plane graphene quantum dots initiated by intense coherent radiation is investigated, using dynamical Hartree-Fock mean-field theory. A microscopic theory describing the extreme nonlinear optical response of plane graphene quantum dots is developed. The closed set of differential equations for the single-particle density matrix at the graphene quantum dots-strong laser field multiphoton interaction is solved numerically. The obtained solutions indicate the significance of the type of edge and lateral size, and bandgap and laser field strength in the high harmonic generation process on the triangular graphene quantum dot.

PACS numbers: 73.21.La, 68.65.-k, 68.65.Pq, 03.65.-w, 32.80.Wr

I. INTRODUCTION

In the last decade, there has been a growing interest to extend high harmonic generation (HHG) to two-dimensional (2D) crystals and nanostructures, such as semimetallic graphene [1], and semiconductor transition metal dichalcogenides [2]. The role of graphene as an effective nonlinear optical material has been discussed in many theoretical [3–20], and experimental [23], [24] studies that consider various extreme nonlinear optical effects, in particular, HHG, which takes place in strong coherent radiation fields in the multiphoton regime at excitation of such nanostructures [25], [26]. On the other hand, apart from the remarkable and unique electronic and optical properties of graphene, the lack of an energy gap as a semimetal greatly limits their applicability, in contrast, for example, to bilayer graphene [27–32].

The problem of a zero energy gap has been solved by decreasing the lateral size of graphene [33]. As a result of dimensional quantization, an energy gap opens. Semimetallic graphene of finite dimensions becomes a semiconductor. Among carbon nanostructures, there are of particular interest as a nonlinear medium the graphene ribbons (nanoribbons) [33], [34], graphene-like quantum dots [21, 22], such as closed-convex fullerenes of different basic symmetry, and the graphene quantum dots (GQDs) of various lateral sizes. The graphene nanostructure can be characterized by whether the sublattice symmetry is reserved. GQD has a gap that can be controlled by their lateral size, shape and type of edge [33]. GQDs behavior is quantitatively different for structures with zigzag and armchair edges, which is related to the edge states present in systems with zigzag edges [36]. So, it is of interest to investigate the HHG process in GQDs with different edges. Such nanostructure exhibits optical properties that are fundamentally different from those of graphene [37–39]. At the same time, carriers in GQD have the same outstanding transport properties as in graphene [3].

The important advantage of GQDs over the graphene

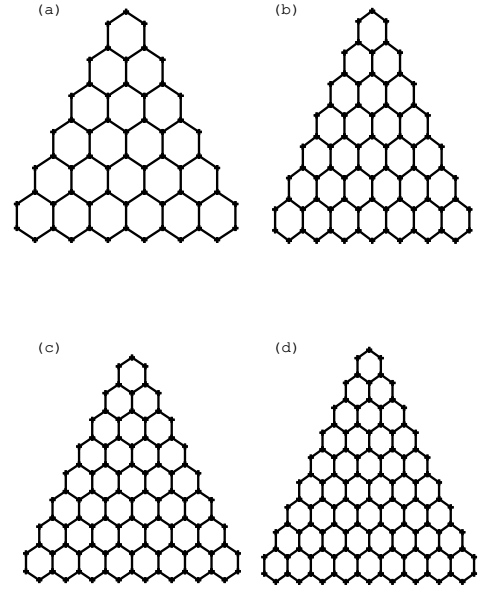


FIG. 1: Schematic plot of the lattice of triangular QGD of zigzag edges with (a–d) $N = 61, 78, 97, 118$ atoms, respectively. The distance between nearest neighboring atoms is $a \simeq 1.42 \text{ \AA}$.

nanoribbons [40] is the limitation of quasiparticles in space. The latter can be crucial for the efficiency of HHG, since the space limitation prevents the propagation of the electron wave packet deposited into also one additional dimension and, therefore, can increase the HHG yield [41].

In the present work, the HHG in triangular GQDs caused by intense coherent radiation is investigated. The closed set of differential equations for the single-particle density matrix at the GQD-strong laser field multiphoton interaction is solved numerically in the scope of the microscopic theory, describing the extreme nonlinear optical response of GQDs is developed. GQD energy gap is controlled by its lateral size, shape, and type of edge.

*Electronic address: amarkos@ysu.am

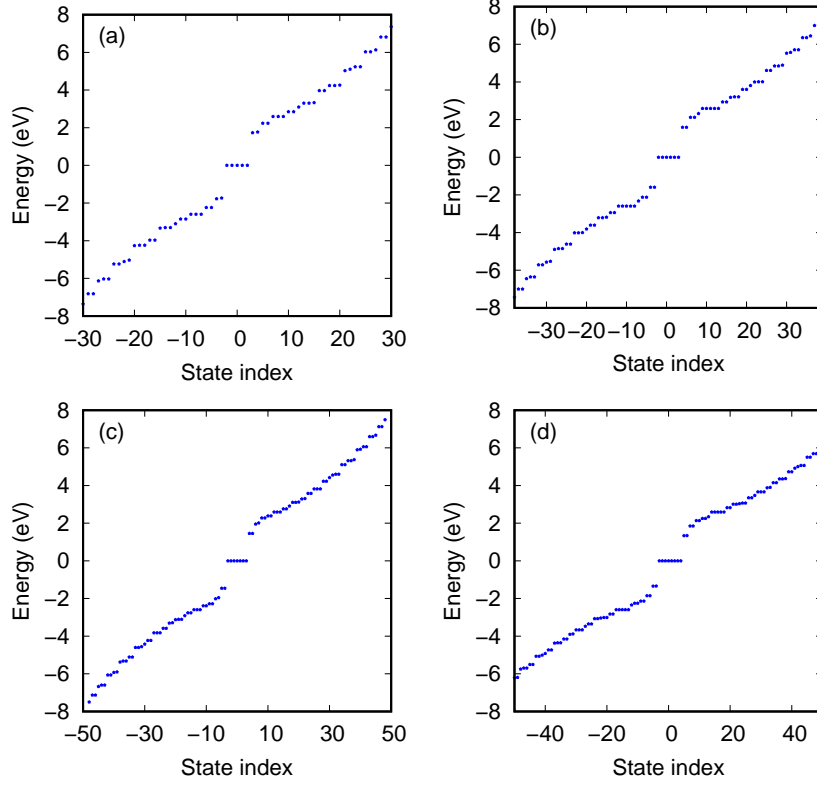


FIG. 2: The eigenenergies in triangular QGD of zigzag edges for (a-d) $N = 61, 78, 97, 118$ atoms, respectively.

The obtained solutions indicate the significance of the lateral size on the HHG process in triangular GQDs type with either armchair or zigzag edge. Thus, we have investigated theoretically the effect of quantum confinement on HHG in GQDs by systematically varying the lateral size of a model dot.

The paper is organized as follows. In Sec. III, the set of equations for the single-particle density matrix is formulated. In Sec. III, we consider multiphoton excitation and generation of harmonics in triangular GQD of the different type of edges and lateral size. Finally, conclusions are given in Sec. IV.

II. DYNAMICAL HARTREE-FOCK MEAN-FIELD THEORY FOR THE HIGH-HARMONIC GENERATION IN QGD

Let a plane GQD placed in the xy plane bounded along the x, y axes, that interacts with a plane quasimonochromatic electromagnetic (EM) wave. We will consider EM wave propagates perpendicular to the xy plane. We assume neutral plane GQDs, which will be described using the empirical tight-binding (TB) model firstly introduced in [42]. Using of the TB model for GQDs were discussed in [33], where the interball hopping is much smaller than the on-ball hopping. TB Hamiltonian can describe finite-size systems by restricting the tunneling

matrix elements t_{ij} to atoms within the quantum dot. The total Hamiltonian can be written as:

$$\hat{H} = \hat{H}_0 + \hat{H}_{\text{int}}. \quad (1)$$

Here

$$\hat{H}_0 = - \sum_{\langle i,j \rangle \sigma} t_{ij} c_{i\sigma}^\dagger c_{j\sigma} + \frac{U}{2} \sum_{i\sigma} \left(c_{i\sigma}^\dagger c_{i\sigma} - \frac{n_i}{2} \right) \left(c_{i\bar{\sigma}}^\dagger c_{i\bar{\sigma}} - \frac{n_i}{2} \right) \quad (2)$$

is the free Hamiltonian of the GQD for TB model, where $c_{i\sigma}^\dagger$ creates an electron with spin polarization σ at site i , and $\langle i, j \rangle$ indicates a summation over nearest neighbor sites with the transfer energy t_{ij} , n_i – average electron density for a site i . The nonzero matrix elements of the TB Hamiltonian given by the first term in (2) correspond to tunneling matrix element t_{ij} between energy states on neighboring sites. The second term in (2) is the electron-electron interaction (EEI) Hamiltonian (\hat{H}_{ee}) in the Hubbard approximation where all Coulomb scattering matrix elements are neglected except for the on-site interaction terms $\sim U$ between spin-up and down electrons occupying the same site i ($\bar{\sigma}$ is the opposite to σ spin polarization). These operators $c_{i\sigma}^\dagger, c_{i\sigma}$ satisfy anticommutation rules: $\{c_{i\sigma}, c_{j\sigma}\} = \{c_{i\sigma}^\dagger, c_{j\sigma}^\dagger\} = 0$, and $\{c_{i\sigma'}, c_{j\sigma}^\dagger\} = \delta_{ij} \delta_{\sigma\sigma'}$, which guarantee antisymmetry of many-particle states.

We assume, that before the interaction: $\langle c_{i\sigma}^\dagger c_{i\sigma} \rangle = n_i$, n_i – total electron density for a site i . In the calculations,

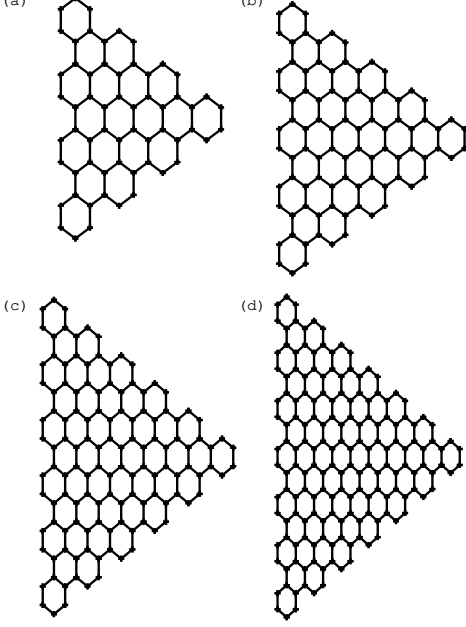


FIG. 3: The same as for Fig. 1 but for triangular QGD of armchair edges. (a-d) respectively correspond to $N = 60, 90, 126, 168$ atoms.

light-matter interaction is described in the length-gauge via pure scalar potential:

$$\hat{H}_{\text{int}} = e \sum_{i\sigma} \mathbf{r}_i \mathbf{E}(t) c_{i\sigma}^\dagger c_{i\sigma},$$

with the elementary charge e , position vector \mathbf{r}_i , and the electric field strength $\mathbf{E}(t)$. In the Hamiltonian we neglect the lattice vibrations. The hopping integral t_{ij} between nearest-neighbor atoms of QGDs can be determined experimentally, and is usually taken to be $t_{ij} = 2.7$ eV [3]. The wave is assumed:

$$E_x(t) = f(t) E_0 \cos \omega t \cos \theta, E_y(t) = f(t) E_0 \cos \omega t \sin \theta, \quad (3)$$

with the frequency ω , pulse envelope $f(t) = \sin^2(\pi t/\mathcal{T})$, the angle θ to the x axis. The pulse duration \mathcal{T} is taken to be 20 wave cycles: $\mathcal{T} = 40\pi/\omega$. From Heisenberg equation $i\hbar \partial \hat{L}/\partial t = [\hat{L}, \hat{H}]$ one can obtain evolutionary equations for the single particle density matrix $\rho_{ij}^{(\sigma)} = \langle c_{j\sigma}^\dagger c_{i\sigma} \rangle$. In addition we will assume that the system relaxes at a rate γ to the equilibrium $\rho_{0ij}^{(\sigma)}$ distribution. To obtain closed set of equations for the single particle density matrix $\rho_{ij}^{(\sigma)} = \langle c_{j\sigma}^\dagger c_{i\sigma} \rangle$, EEI will be considered under the Hartree-Fock approximation:

$$\hat{H}_{ee}^{HF} \simeq \frac{U}{2} \sum_{i\sigma} \left(\langle c_{i\sigma}^\dagger c_{i\sigma} \rangle - \frac{n_i}{2} \right) \left(c_{i\sigma}^\dagger c_{i\sigma} - \frac{n_i}{2} \right). \quad (4)$$

Thus, we obtain the following equation for the density matrix:

$$i\hbar \frac{\partial \rho_{ij}^{(\sigma)}}{\partial t} = \sum_k \left(t_{kj} \rho_{ik}^{(\sigma)} - t_{ik} \rho_{kj}^{(\sigma)} \right) + U \left(\rho_{ii}^{(\sigma)} - \rho_{jj}^{(\sigma)} \right) \rho_{ij}^{(\sigma)} + e \mathbf{E}(t) (\mathbf{r}_i - \mathbf{r}_j) \rho_{ij}^{(\sigma)} - i\hbar \gamma \left(\rho_{ij}^{(\sigma)} - \rho_{0ij}^{(\sigma)} \right). \quad (5)$$

We numerically diagonalize the tight-binding Hamiltonian \hat{H}_0 . For a half-filled system, the static Hartree-Fock Hamiltonian vanishes $\hat{H}_{ee}^{HF} \simeq 0$. It should be mentioned that EEI in Hartree-Fock limit is included in empirical hopping integral between nearest-neighbor atoms t which is chosen to be close to experimental values. Thus, on-site EEI in the Hartree-Fock approximation is relevant for the quantum dynamics initiated by the pump laser field and as we will see below considerably modifies the HHG spectrum. With the numerical diagonalization, we find eigenstates $\psi_\mu(i)$ and eigenenergies ε_μ ($\mu = 0, 1, \dots, N-1$). The results of numerical diagonalization are shown in Fig. 2, 4. Without tunneling all energy levels were degenerate, $\psi_\mu(i) = 0$. So, the tunneling removed the degeneracy and led to the formation of the band of 1–2 valence states below the Fermi level, a band of 1–2 conduction states above the Fermi level, $\varepsilon_\mu = 0$, and a gap across the Fermi level (see also [33]). The quantum dynamics of strong field periodically driven QGD is governed by a closed set of differential equations (5), which should be solved with the proper initial conditions. We construct initial a density matrix $\rho_{0ij}^{(\sigma)}$ via the filling of electron states in the valence band according to the Fermi–Dirac-distribution. Since the energy gap is large enough we assume Fermi–Dirac-distribution at zero temperature:

$$\rho_{0ij}^{(\sigma)} = \sum_{\mu=N/2}^{N-1} \psi_\mu^*(j) \psi_\mu(i).$$

III. NUMERICAL RESULTS FOR HHG EFFICIENCY IN TRIANGULAR QGDS

The HHG spectrum is evaluated from the Fourier transformation $\mathbf{a}(\Omega)$ of the dipole acceleration $\mathbf{a}(t) = d^2 \mathbf{d}/dt^2$. The dipole is defined as $\mathbf{d}(t) = \langle \sum_{i\sigma} \mathbf{r}_i c_{i\sigma}^\dagger c_{i\sigma} \rangle$. For convince we normalize the dipole acceleration by the factor $a_0 = \varpi^2 \bar{d}$, where $\varpi = 1$ eV/ \hbar and $\bar{d} = 1$ Å. The power radiated at the given frequency is proportional to $|\mathbf{a}(\Omega)|^2$. In order to clarify the main aspects of HHG in triangular QGDs, we assume the excitation frequency is $\omega = 0.1$ eV/ \hbar , that is much smaller than the typical gap $U \simeq 3$ eV. The relaxation rate is taken to be $\hbar\gamma = 50$ meV. For the most calculations, the wave (3) is assumed to be linearly polarized along the x axis ($\theta = 0$). The x axis is in the plane of Figs. 1, 3, and is directed along x to the right.

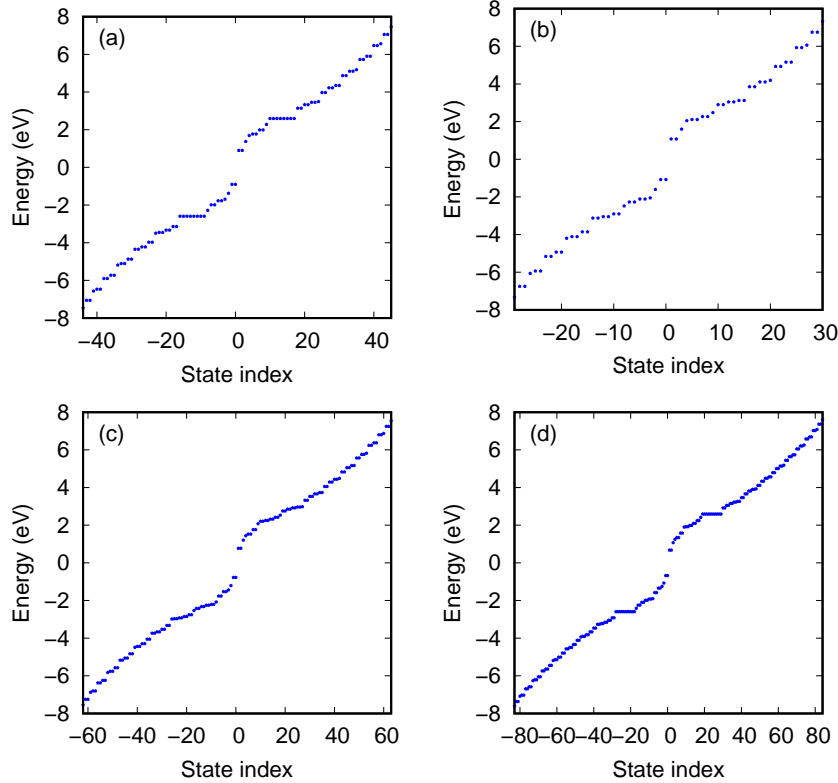


FIG. 4: The same as for Fig. 2 but for triangular QGD of armchair edges. (a–d) respectively correspond to $N = 60, 90, 126, 168$ atoms.

Figs. 1, 3 demonstrate schematically a graphene lattice, and Figs. 2, 4 show TB energy spectrum in the vicinity of the Fermi level, $\varepsilon_\mu = 0$, for a triangular QGD with zigzag and armchair edges for the different numbers of carbon atoms. As it is shown in Figs. 1–4, with an increase in the number of lattice atoms, the density of eigenstates increases. As will be seen later, this will increase the probabilities of multiphoton HHG.

To compare the HHG radiation spectra in the triangular GQDs with different edges at different numbers of lattice atoms, in further figures we have plotted all results for the spectra via the normalized atom number N . In Fig. 5 plotted the components $|a_x(\Omega)|$ and $|a_y(\Omega)|$ in the strong EM wave with the amplitude $E_0 = 0.3$ B /Å, and the EEI energy $U \simeq 3$ eV. As shown in this figure, in a strong laser field, multiphoton harmonics are significant, and the HHG yields for GQDs are equally significant for both armchair and zigzag edges, especially for large N . In both cases, the HHG spectra have a multistep plateau structure, which is associated with the excitations of energy eigenstates between the unoccupied energy levels and the occupied level [33]. GQD with armchair-like edges has axial symmetry (see Fig. 3), and, in particular, in this case $|a_y| = 0$ (therefore, it is absent in Fig. 5), while in the case of zigzag edges both components $|a_x|$ and $|a_y|$ are essential (fig. 5). In addition, only odd harmonics are visible in the

HHG spectrum in armchair-shaped GQDs, as in ordinary graphene [1]. However, for zigzag edges, due to the absence of inversion symmetry, both odd and even harmonics are present in the HHG emission spectrum. To show this clearly, in Fig. 6 separately shows the results for HHG for the first thirty harmonics with approximately the same number ($N \simeq 60$) of atoms of a triangular GQD with different edges.

Next, we consider the HHG spectra as a function of pump wave intensity. Fig. 7 demonstrates the HHG spectra as a function of EM field amplitude and the harmonic order for a fixed EEI energy $U = 3$ eV. To compare in Fig. 7a, c and Fig. 7b, d we will investigate the QGDs with a similar number of carbon atoms but different border edges. As shown in Fig. 7, the HHG probability increases either with an increase in the number N of dots' particles or with an arise more new energy states (also see Figs. 1–4). The cutoff harmonic linearly increases with increasing the field strength. Then, reaching the harmonic n_{cut} which corresponds to the transition of the lowest occupied energy state to the highest unoccupied one, the HHG rate is saturated (stepped yellow envelope). The harmonic cutoff number can be seen in Fig. 5: $n_{\text{cut}} \simeq 160$. Note that linear dependence of the cutoff harmonics on the field strength is inherent to HHG via discrete levels, or in crystals with linear energy dispersion. As in atomic cases for QGD with the increase

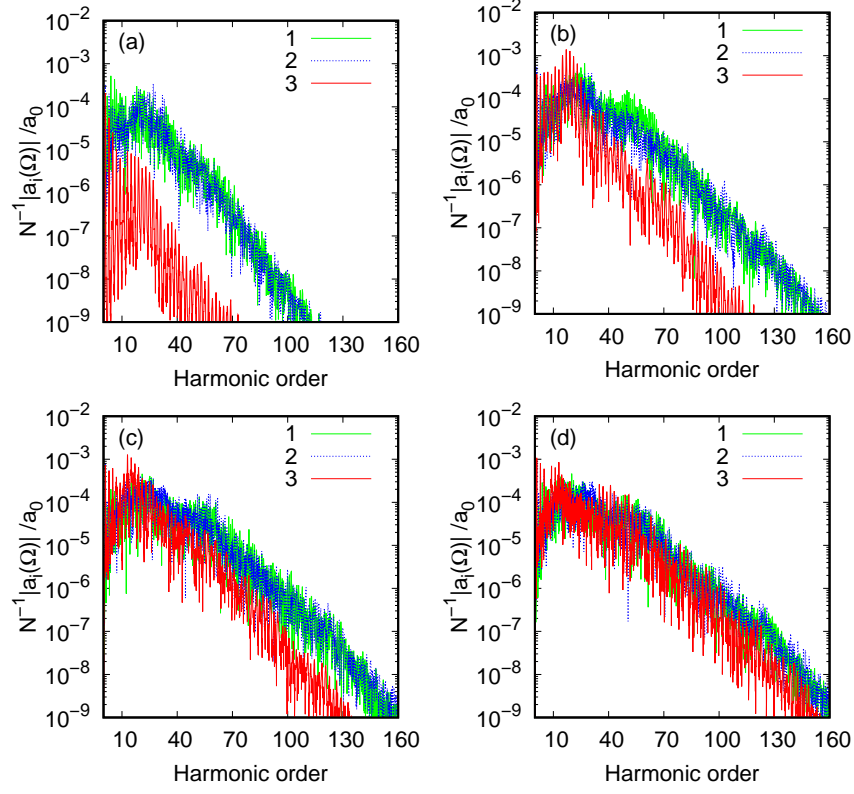


FIG. 5: (Color online) The HHG emission rate represents via dipole acceleration Fourier transformation $N^{-1}|a_i(\Omega)|/a_0$ in the logarithmic scale versus the harmonic number for triangular QGD. (1) presents the components $|a_x|$ with zigzag and (3) armchair edges; (2) $|a_y|$ with zigzag edges. (a–d) for (1, 2) correspond to $N = 61, 97, 118, 141$ atoms, and (a–d) for (3) correspond to $N = 60, 90, 126, 168$ atoms. The EM wave is assumed to be linearly polarized along x axis. The wave frequency is $\omega = 0.1 \text{ eV}/\hbar$ and field strength is $E_0 = 0.3 \text{ V}/\text{\AA}$. The spectra are shown for moderate (typical) EEI energy: $U = 3 \text{ eV}$. The relaxation rate is $\hbar\gamma = 50 \text{ meV}$.

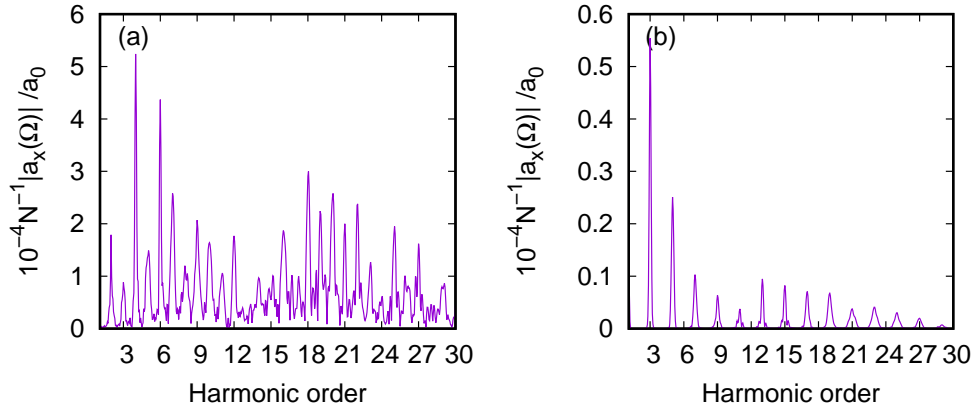


FIG. 6: (Color online) The same as for Fig. 5 but without the logarithmic scale. (a) shows harmonics (even and odd) in a triangular GQD with zigzag edges for $N = 60$ atoms, (b) – harmonics (only odd) in a GQD with armchair edges for $N = 61$ atoms.

of the pump wave strength at a fixed photon energy the cutoff harmonic energy ($\hbar\omega N_{\text{cut}}$) is increased.

Besides, as was shown in [29] the on-site EEI suppresses the charge fluctuation and reduces the absorbed energy. Suppression of HHG yields due to EEI is also

expected. The latter is shown in Fig. 8, where the HHG spectra in the strong EM field regime versus photon number and EEI energy are shown for different border edges and carbon atom numbers. As can be seen from Fig. 8, for a small number of N GQD atoms with an increase

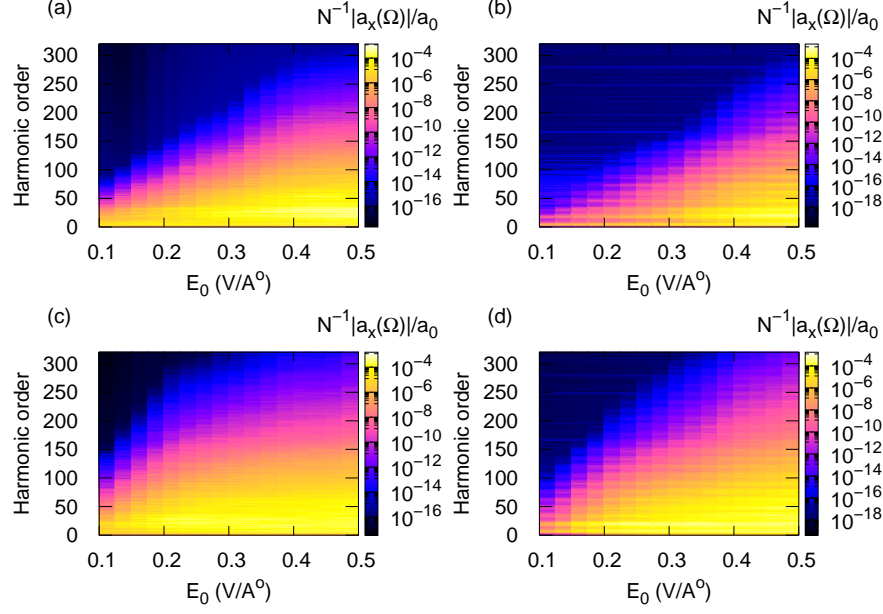


FIG. 7: (Color online) The color bar represents the HHG emission rate via dipole acceleration Fourier transformation $N^{-1}|a_x(\Omega)|/a_0$ in strong field regime in the logarithmic scale versus harmonic order and EM field amplitude for triangular QGD of different edges and carbon atom numbers. (a, c) correspond to atom numbers $N = 61$ and $N = 118$ for QGD with zigzag edges, (b, d) correspond to atom numbers $N = 60$ and $N = 126$ for QGD with armchair edges. The wave is assumed to be linearly polarized along x axis. The wave frequency is $\omega = 0.1$ eV/ \hbar and the EEI energy: $U = 3$ eV. The relaxation rate is $\hbar\gamma = 50$ meV.

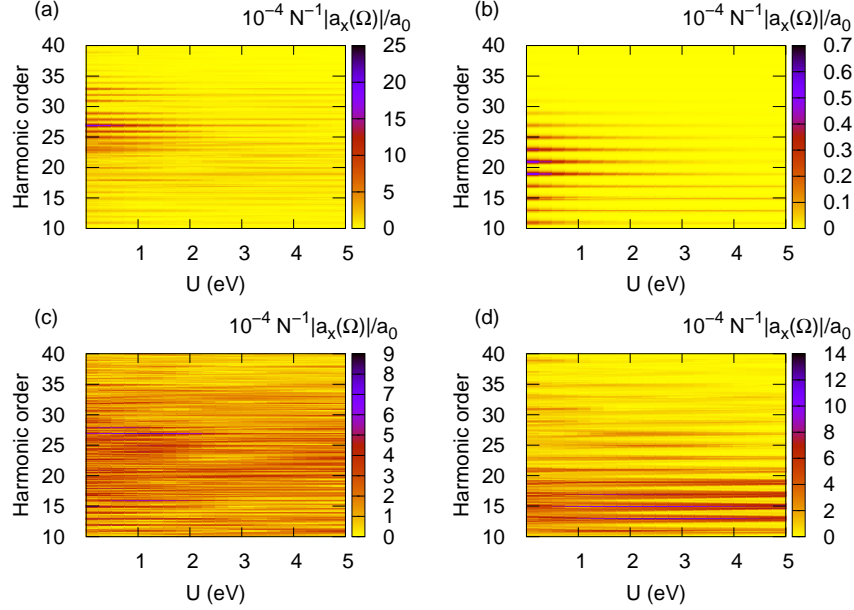


FIG. 8: (Color online) The same as in Fig. 7 but without the logarithmic scale, versus EEI energy and harmonic order at fixed EM field strength $E_0 = 0.3$ V/ \AA .

the EEI energy, the HHG rate is generally suppressed (therefore, Fig. 8 shows the dependence for mean harmonics with numbers < 40). The latter is not the case for large N , when the density of energy states increases (Fig. 8c, d). The HHG spectrum ceases to depend on

the Coulomb EEI. This property is inherent in ordinary graphene [1], unlimited in space.

We also investigated the HHG spectra dependence versus the EM wave strength orientation. In Fig. 9 we plot the HHG spectra versus the photon number and

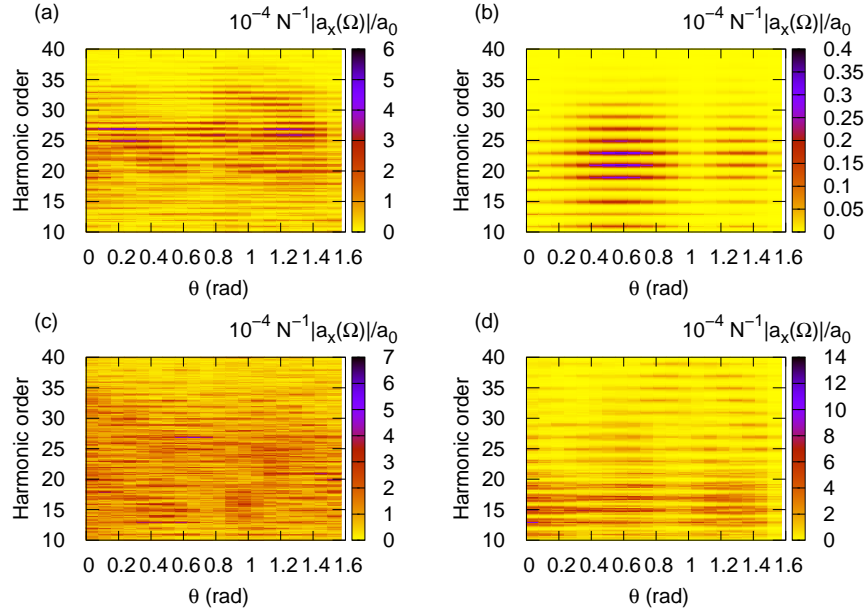


FIG. 9: (Color online) The HHG emission rate via dipole acceleration Fourier transformation $N^{-1}|a_x(\Omega)|/a_0$ versus harmonic order and angle θ of the intensity of the EM field with the x axis. (a, c) correspond to the number of atoms $N = 61$ and $N = 118$ for a triangular GQD with zigzag edges, (b, d) correspond to the number of atoms $N = 60$ and $N = 126$ for a triangular GQD with armchair edges. The wave frequency is $\omega = 0.1$ eV/ \hbar , the field strength is $E_0 = 0.3$ V/ \AA , the EEI energy is $U = 3$ eV. The relaxation rate is $\hbar\gamma = 50$ meV.

pump wave strength orientation under x axis for a given strength ($E_0 = 0.3$ V/ \AA) and frequency and for moderate EEI energy $U = 3$ eV. As can be seen from Fig. 9, the orientation of the pump wave at different angles to the x axis leads to different harmonic spectra. This is due to the fact that the triangular GQD has no inversion symmetry (see Fig. 1-4). As shown in fig. 9a, b for angles $0 < \theta < \pi/2$ the rate of middle harmonics (maxima for numbers $\simeq 10 - 40$) increases, and higher harmonics are suppressed. However, in Fig. 9c, d, it can be seen that with an increase in the density of energy states, this regularity is violated, and the HHG spectrum ceases to depend on the orientation of the EM wave force. By this, the GQD becomes similar to graphene unbounded in space [1].

IV. CONCLUSION

We have studied the influence of intense coherent radiation on GQDs. The microscopic theory has been developed to describe the extreme nonlinear optical response of the triangular GQDs. A closed system of differential equations for a one-particle density matrix in the multiphoton interaction of a GQD with a strong laser field is solved numerically. The solutions obtained indicate the importance of the type of edge and lateral size, as well as the significance of the bandgap and the magnitude of the laser field for the HHG process in plane GQDs. The harmonic cutoff number increases linearly

with increasing field strength. As in the case of HHG on atoms, for a GQD, with an increase the pump wave strength at fixed photon energy, the harmonic cutoff energy ($\hbar\omega n_{\text{cut}}$) increases linearly. Due to the absence or presence of symmetry of the sublattice in a triangular GQD with zigzag edges, harmonics of both odd and even order appear during the generation in the field of an EM wave, when only odd harmonics are significant for armchair edges. We also investigated the HHG spectra dependence versus the pump wave strength orientation. As the numerical results show, due to the difference in the symmetry of the sublattice, the same angles give different partial yields in the HHG spectra for triangular GQDs with armchair and zigzag edges. In addition, the rate of middle harmonics for a small number of atoms increases, while higher harmonics are suppressed, which is not the case with an increase in the density of energy states. In addition, with an increase in the density of energy states, the rule is violated when, in the case of a small number of GQD atoms, with an increase in the EEI energy, the HHG rate is generally suppressed. Thus, with an increase in the average the density of eigenstates of the GQD behaves like graphene unbounded in space. So, we investigated the size and shape of the GQD using quasiparticle confinement in space. The results obtained show that GQDs can serve as an effective medium for the generation of even and odd high-order harmonics when interacting with a laser field of moderate intensity due to the limitation of quasiparticles in the GQD. In addition, the HHG probability increases with an increase in

the number of GQD atoms or with the appearance of new energy states. This is a potential way to increase the quantum yield and photon energy during HHG in graphene-like quantum dots.

Acknowledgments

The authors are deeply grateful to prof. H. K. Avetissian and Dr. G. F. Mkrtchian for permanent discussions

and valuable recommendations. The work was supported by the Science Committee of RA in frames of the research project 20TTWS-1C010.

-
- [1] K. S. Novoselov, A. K. Geim, S. V. Morozov et al., *Science* **306**(5696), 666 (2004).
 - [2] H. Liu, Y. Li, Y. S. You, S. Ghimire, T. F. Heinz, D. A. Reis, *Nat. Phys.* **13**, 262 (2017).
 - [3] A. H. C. Neto, F. Guinea, N. M. R. Peres et al., *Rev. Mod. Phys.* **81**, 109 (2009).
 - [4] S. A. Mikhailov, K. Ziegler, *J. Phys. Condens. Matter* **20**, 384204 (2008).
 - [5] H. K. Avetissian, G. F. Mkrtchian, K. V. Sedrakian et al., *J. Nanophoton.* **6**, 061702 (2012).
 - [6] H. K. Avetissian, G. F. Mkrtchian, K. G. Batrakov et al., *Phys. Rev. B* **88**, 165411 (2013).
 - [7] I. Al-Naib, J. E. Sipe, M. M. Dignam, *New J. Phys.* **17**, 113018 (2015).
 - [8] L. A. Chizhova, F. Libisch, J. Burgdorfer, *Phys. Rev. B* **94**, 075412 (2016).
 - [9] L. A. Chizhova, F. Libisch, J. Burgdorfer, *Phys. Rev. B* **95**, 085436 (2017).
 - [10] H. K. Avetissian, A. G. Ghazaryan, G. F. Mkrtchian, Kh. V. Sedrakian, *J. Nanophoton.* **11**, 016004 (2017).
 - [11] D. Dimitrovski, L. B. Madsen, T. G. Pedersen, *Phys. Rev. B* **95**, 035405 (2017).
 - [12] H. K. Avetissian, G. F. Mkrtchian, *Phys. Rev. B* **97**, 115454 (2018).
 - [13] H. K. Avetissian, A. K. Avetissian, B. R. Avchyan, G. F. Mkrtchian, *Phys. Rev. B* **100**, 035434 (2019).
 - [14] H. K. Avetissian, G. F. Mkrtchian, *Phys. Rev. B* **99**, 085432 (2019).
 - [15] A. K. Avetissian, A. G. Ghazaryan, Kh. V. Sedrakian, *J. Nanophoton.* **13**, 036010 (2019).
 - [16] H. K. Avetissian, A. K. Avetissian, A. G. Ghazaryan et al., *J. Nanophoton.* **14**, 026004 (2020).
 - [17] A. G. Ghazaryan, H. H. Matevosyan, and Kh. V. Sedrakian, *J. Nanophoton.* **14**, 046009 (2020).
 - [18] H. K. Avetissian, *Relativistic nonlinear electrodynamics, The QED vacuum and matter in super-strong radiation fields*, Springer, Berlin (2016).
 - [19] B. R. Avchyan, A. G. Ghazaryan, K. A. Sargsyan, Kh. V. Sedrakian, *JETP* **132**(6), 883 (2021).
 - [20] A. G. Ghazaryan, *JETP* **132**(5), 843 (2021).
 - [21] G. P. Zhang, Y. H. Bai, *Phys. Rev. B* **101**, 081412(R) (2020).
 - [22] H. K. Avetissian, A. G. Ghazaryan, G. F. Mkrtchian, arXiv preprint arXiv:2108.05352 (2021).
 - [23] P. Bownan, E. Martinez-Moreno, K. Reimann et al., *Phys. Rev. B* **89**, 041408(R) (2014).
 - [24] N. Yoshikawa, T. Tamaya, K. Tanaka, *Science* **356**, 736 (2017).
 - [25] H. K. Avetissian, A. K. Avetissian, G. F. Mkrtchian, Kh. V. Sedrakian, *Phys. Rev. B* **85**, 115443 (2012).
 - [26] A. K. Avetissian, A. G. Ghazaryan, Kh. V. Sedrakian, B. R. Avchyan, *J. Nanophotonics* **12**, 016006 (2018).
 - [27] E. V. Castro, K. S. Novoselov, S. V. Morozov et al., *Phys. Rev. Lett.* **99**, 216802 (2007).
 - [28] J. B. Oostinga, H. B. Heersche, X. Liu et al., *Nature Materials* **7**, 151 (2008).
 - [29] Y. B. Zhang, T.-T. Tang, C. Girit et al., *Nature* **459**, 820 (2009).
 - [30] F. Guinea, A. H. C. Neto, N. M. R. Peres, *Phys. Rev. B* **73**, 245426 (2006).
 - [31] M. Koshino, T. Ando, *Phys. Rev. B* **73**, 245403 (2006).
 - [32] A. Varleta, M. Mucha-Kruczynski, D. Bischoff et al., *Synthetic Metals* **210**, 19 (2015).
 - [33] A. D. Guclu, P. Potasz, M. Korkusinski, P. Hawrylak, *Graphene Quantum Dots*, Springer, Berlin (2014).
 - [34] H. K. Avetissian, B. R. Avchyan, G. F. Mkrtchian, K. A. Sargsyan, *J. Nanophoton.* **14**, 026018 (2020).
 - [35] A. D. Guclu, P. Potasz, P. Hawrylak, *Graphene-based integrated electronic, photonic and spintronic circuit, invited paper, in Future Trends in Microelectronics*, Wiley, New York, (2013).
 - [36] A. D. Guclu, P. Potasz, P. Hawrylak, *Phys. Rev. B* **82**, 155445 (2010).
 - [37] A. D. Guclu, P. Potasz, O. Voznyy et al., *Phys. Rev. Lett.* **103**, 246805 (2009).
 - [38] O. Voznyy, A. D. Guclu, P. Potasz, P. Hawrylak, *Phys. Rev. B* **83**, 165417 (2011).
 - [39] W. L. Wang, S. Meng, E. Kaxiras, *Nano Lett.* **8**, 241 (2008).
 - [40] M. Y. Han, B. Ozyilmaz, Y. Zhang, Ph. Kim, *Phys. Rev. Lett.* **98**, 206805 (2007).
 - [41] M. Lewenstein, Ph. Balcou, M. Y. Ivanov et al., *Phys. Rev. A* **49**, 2117 (1994).
 - [42] P. R. Wallace, *Phys. Rev.* **71**, 622 (1947).